# 20 m Annual Paddy Rice Area Map for Mainland Southeast Asia Using Sentinel-1 SAR Data

Chunling Sun[1,2,3], Hong Zhang[1,2,3*], Lu Xu[1,2], Ji Ge[1,2,3], Jingling Jiang[1,2,3], Lijun Zuo[1,2], Chao Wang[1,2,3]

[1]Key Laboratory of Digital Earth Science, Aerospace Information Research Institute, Chinese Academy of Sciences, Beijing 100094, China
[2]International Research Center of Big Data for Sustainable Development Goals, Beijing 100094, China
[3]College of Resources and Environment, University of Chinese Academy of Sciences, Beijing 100049, China

*Correspondence to*: Hong Zhang (zhanghong@radi.ac.cn)

**Abstract.** Over 90% of the world's rice is produced in the Asia-Pacific Region. Synthetic aperture radar (SAR) enables all-day and all-weather observations of rice distribution in tropical and subtropical regions. The complexity of rice cultivation patterns in tropical and subtropical regions makes it difficult to construct a representative data-relevant rice crop model, increasing the difficulty of extracting rice distributions from SAR data. To address this problem, a rice area mapping method for large regional tropical or subtropical areas based on time-series Sentinel-1 SAR data is proposed in this study. Based on the analysis of rice backscattering characteristics in mainland Southeast Asia, the combination of spatio-temporal statistical features with good generalization ability was selected and then input into the U-Net semantic segmentation model, combined with WorldCover data to eliminate false alarms, finally the 20-meter resolution rice area map of five countries in mainland Southeast Asia in 2019 was obtained. The proposed method achieved an accuracy of 92.20% on the validation sample set, and the good agreement was obtained when comparing our rice area map with statistical data and other rice area maps at the national and provincial levels. The maximum coefficient of determination R2 was 0.93 at the national level and 0.97 at the provincial level. These results demonstrate the advantages of the proposed method in rice area mapping with complex cropping patterns and the reliability of the generated rice area maps. The 20 m annual paddy rice area map for mainland Southeast Asia is available at https://doi.org/10.5281/zenodo.7315076(Sun et al., 2022b).

## 1 Introduction

Sustainable development Goal 2 "Zero Hunger" was set by the United Nations in 2015(Desa, 2016). The dual pressure of population and environment threatens the sustainability of global food security(Faostat, 2010; Godfray et al., 2010). Rice feeds more than half of the world's population as a staple food and is a major crop for world food security (Kuenzer and Knauer, 2012). Asia is the largest rice-producing region in the world (Chen et al., 2012), and Southeast Asia accounts for 40% of global rice exports(Yuan et al., 2022). High-precision rice planting area maps are the basis for monitoring rice growth and forecasting yields, the cornerstone for the government, planners and policymakers to formulate reasonable policies, and the guarantee of

global food security(Mosleh et al., 2015; Laborte et al., 2017; Clauss et al., 2018; Jin et al., 2018; Yu et al., 2020; Hoang-Phi et al., 2021).

Remote sensing technology plays a crucial role in rice growth monitoring and distribution mapping (Weiss et al., 2020; Zhao et al., 2021; Tsokas et al., 2022). Rice area mapping at the national scale usually uses medium- and low-resolution optical remote sensing data, such as MODIS and Landsat data. Some researchers used MODIS multitemporal data to produce rice area maps of China with resolutions of 500 m, 500 m, 250 m and 500 m respectively (Xiao et al., 2005; Sun et al., 2009; Clauss et al., 2016; Qiu et al., 2022). Guan et al. produced rice area maps of Vietnam at 500 m resolution using MODIS time series data in 2010(Guan et al., 2016). The National Agricultural Statistics Service (NASS) released the state-based Crop Data Layer (CDL), a 30-m resolution crop distribution map product for the entire continental United States, using multisource medium resolution remote sensing data (Landsat, IRS-p6, DEIMOS-1, etc.)(Johnson and Mueller, 2010) .Luo et al. and Wei et al. used Landsat time-series data to produce 1 km and 30 m resolution rice datasets for China, respectively (Luo et al., 2020; Wei et al., 2022). Recently， the Sentinel -2 satellite sensor opens up new possibilities for paddy rice monitoring. Liu et al. obtained medium-resolution rice area maps of China using Sentinel-2 time series data in 2020 (Liu et al., 2022).

At the continental scale, MODIS time-series data were frequently used to map the distribution of rice cultivation (Dong et al., 2016a; Dong et al., 2016b). Xiao et al., Gumma et al. and Bridhikitti et al. produced low- and medium-resolution rice area maps for several South and Southeast Asian countries using MODIS data at the 500 m spatial resolution, respectively (Xiao et al., 2006; Gumma et al., 2011a; Gumma et al., 2011b; Bridhikitti and Overcamp, 2012; Gumma et al., 2014). Nelson and Gumma extracted the 500 m spatial resolution general rice extent map in Asia from 2000 to 2012 using MODIS data (Nelson and Gumma, 2015). Using MODIS time-series data, Zhang et al. generated rice acreage maps for China and India from 2000 to 2015 (Zhang et al., 2017). Han et al. used MODIS data to complete 500 m annual rice maps for the Asian monsoon region from 2000 to 2020(Han et al., 2022). SPOT data were also used for continent-wide rice area mapping. Manjunath et al. used 2009-2010 multi-temporal SPOT VGT normalized difference vegetation index (NDVI) data to produce 1km resolution rice area maps for South and Southeast Asia(Manjunath et al., 2015).

Most of the rice in the world is distributed in hot and rainy areas. However, optical data are easily obscured by clouds, which also poses a challenge for rice area extraction in humid and sub-humid climates with abundant water resources such as Southeast Asia(Liu et al., 2019; Sun et al., 2021). Compared with traditional optical remote sensing, synthetic aperture radar (SAR) is an active microwave radar with the advantages of all-day and all-weather, which is weather-independent and can penetrate clouds, and is very sensitive to the geometric structure and dielectric properties of crops(Huang et al., 2017; Orynbaikyzy et al., 2019; Sun et al., 2022a). In recent years, free SAR data represented by Sentinel-1 data have been widely used in rice mapping over large regions. Singha et al. obtained seasonal rice maps at 10 m resolution for Bangladesh and northeast India using time-series Sentinel-1VH data for 2017 (Singha et al., 2019). Pan et al. used 2016-2020 Sentinel-1VH data to produce 10-m spatial resolution double-season rice maps for nine provinces in southern China (Pan et al., 2021). Xu et al. used time-series Sentinel-1VH data to obtain a 20 m rice area map for Thailand in 2019 (Xu et al., 2021).

To take full advantage of multi-source remote sensing data, some researchers combined optical and SAR time-series data in the large-scale rice mapping studies (Thenkabail et al., 2009; Zhang et al., 2018; You and Dong, 2020). Phan et al. used Sentinel 1/2 and Landsat data to produce the first Vietnam land use/land cover annual dataset with 30m resolution from 1990 to 2020 (Phan et al., 2021). Han et al. obtained 500m resolution rice maps from 2017 to 2019 in Northeast and Southeast Asia using Sentinel-1 and MODIS time-series data (Han et al., 2021).

At present, large-scale rice mapping methods based on remote sensing data can be divided into two categories, one is the combination of phenological information and remote sensing images, and the other is the combination of time series data and machine learning relying on image information. The phenology-based approach refers to the extraction of rice by defining phenological indicators or identifying rice growing stages by combining the time-series data covering the rice growth cycle and the analysis of rice phenological calendar (Nelson et al., 2014; Chen et al., 2016; Nguyen and Wagner, 2017; Liu et al., 2018; Xin et al., 2020; Ni et al., 2021). The growing stages such as transplanting, heading and maturity are most often used to extract rice. Shew et al. combined vegetation indices extracted from Landsat time-series data with a rule-based algorithm for growing stages to map a 30 m dry season rice map of Bangladesh from 2014 to 2018 (Shew and Ghosh, 2019). Li et al. extracted the minimum and maximum values of permanent water backscatter coefficients and three thresholds of phenological characteristics, namely, the date of the beginning of the season, date of maximum backscatter during the peak growing season, and length of the vegetative stage from 402 scenes of Sentinel-1 data in 2017 to map rice paddies in the Mun River basin ,Thailand (Li et al., 2020).Kang et al. completed a 10 m resolution rice map of Cambodia from Sentinel-1 (2015) and Sentinel-2 (2015-2017) time-series data using three key rice phenological periods in the dry and rainy seasons, respectively (Kang et al., 2022).

However, the phenology-based methods rely too much on human intervention and are not suitable for rice area extraction with complex cropping cycles. The approaches based on the combination of time series data and machine learning method refer to the direct use of time series as the input features for machine learning (Ndikumana et al., 2018; Chang et al., 2020; Mansaray et al., 2021; Yang et al., 2021). Machine learning methods are used to extract rice information by mining fixed relationships across growth periods of rice (Yang et al., 2019; You et al., 2021). Torbick et al. used Sentinel-1, Landsat-8 and PALSAR-2 time series data and a random forest algorithm to map rice planting area and planting intensity of Myanmar with 20 m resolution in 2015 (Torbick et al., 2017). Inoue et al. developed a 30 m resolution map of paddy rice in Japan for 2018 using Sentinel-1 SAR data and Sentinel-2 data with the conventional decision tree methods (Inoue et al., 2020). Wei et al. completed rice area mapping for the Arkansas River Basin, USA, by entering dual-polarized Sentinel-1 data from 2017-2019 into a modified U-Net model (Wei et al., 2021). Soh et al. used Sentinel-1 and Sentinel-2 time series data and a K-means clustering method to map rice in West Malaysia (Soh et al., 2022).

The climate in tropical or subtropical regions such as Southeast Asia is suitable for rice growth throughout the year, increasing the difficulty of extracting information on the distribution of rice areas. First, it is difficult to obtain accurate phenological information, as the climate in Southeast Asia is hot and humid for rice growth, the timing of rice seedling and transplanting is more flexible (Xu et al., 2021). Thus, it is difficult to determine effective phenological indicators and accurately identify rice

growing stages. Second, rice cultivation patterns in Southeast Asia are too complex to construct a representative rice growth model (Kang et al., 2022). This poses obstacles for rice area extraction methods that utilize time-fixed relationships in time-series data.

Current publicly downloadable remote sensing data-based rice products for Southeast Asia include the Asia rice map (IRRI Rice Data, 500 m) (Nelson and Gumma, 2015), Vietnam-wide annual land use/land cover datasets from 1990 to 2020 (VLUCD, 30 m) (Phan et al., 2021), annual paddy rice maps for Northeast and Southeast Asia from 2017 to 2019 (NESEA-Rice10, 10 m) (Han et al., 2021), and annual rice in the Asian monsoon region from 2000 to 2020 (500 m) (Han et al., 2022). Except for Vietnam's VLUCD, the source data for the public rice maps in Southeast Asia were mainly MODIS. Rice area maps using MODIS data contained a large number of mixed pixels due to low spatial resolution (Dong et al., 2015; Shew and Ghosh, 2019), which affected the accuracy of rice area maps.

Therefore, in this study, to meet the requirements of high-precision rice area mapping in Southeast Asia, the objectives accomplished using Sentinel-1 time-series data are as follows.

(1) A new feature extraction method is proposed by analyzing the time-series backscattering variation of rice in mainland Southeast Asia. The method does not need to summarize the general evolutionary model from rice backscatter coefficients with diverse cultivation patterns. Using three simple but effective temporal statistical features defined in this study, it is possible to capture features that provide key information about the rice growth process. This study provides a new idea for rice area mapping methods in tropical or subtropical regions.

(2) A deep combination of the above features and the U-Net model will be used to fully exploit the pixel-level semantic features to complete the annual rice area mapping of five Southeast Asian countries in 2019, enriching the available Southeast Asian rice area maps, and providing support information for the scientific community and scientific decision-making.

The rest of the paper is organized as follows. Section 2 describes the study area and the data information used; Section 3 presents the rice area mapping scheme; Section 4 presents the rice area mapping results and accuracy assessment; Section 5 discusses the results; Section 6 gives the data addresses and Section 7 draws conclusions.

## 2 Materials

### 2.1 Study area

Approximately 90% of the world's rice is grown on 140 million hectares of land in Asia. The rice production in mainland Southeast Asian accounts for about 15% of the world rice production(Fao, 2020). The study area is five countries in mainland Southeast Asia, namely, Myanmar, Thailand, Laos, Cambodia, and Vietnam, as shown in Figure 1. These countries have more land under rice cultivation than any other crop. And Vietnam and Thailand are the two largest rice exporters in the world (Yuan et al., 2022). Indeed, changes in rice production in these countries could destabilize international rice markets and have a clear impact on global food security.

Southeast Asia has a tropical monsoon climate with an average annual temperature of 20-27 °C and abundant rainfall. Therefore, rice can be grown at any time of the year. Agricultural systems in Southeast Asia are dominated by rainfed lowland rice and irrigated lowland rice (Kuenzer and Knauer, 2012). Under suitable irrigation conditions, rice can be harvested two to three times per year.

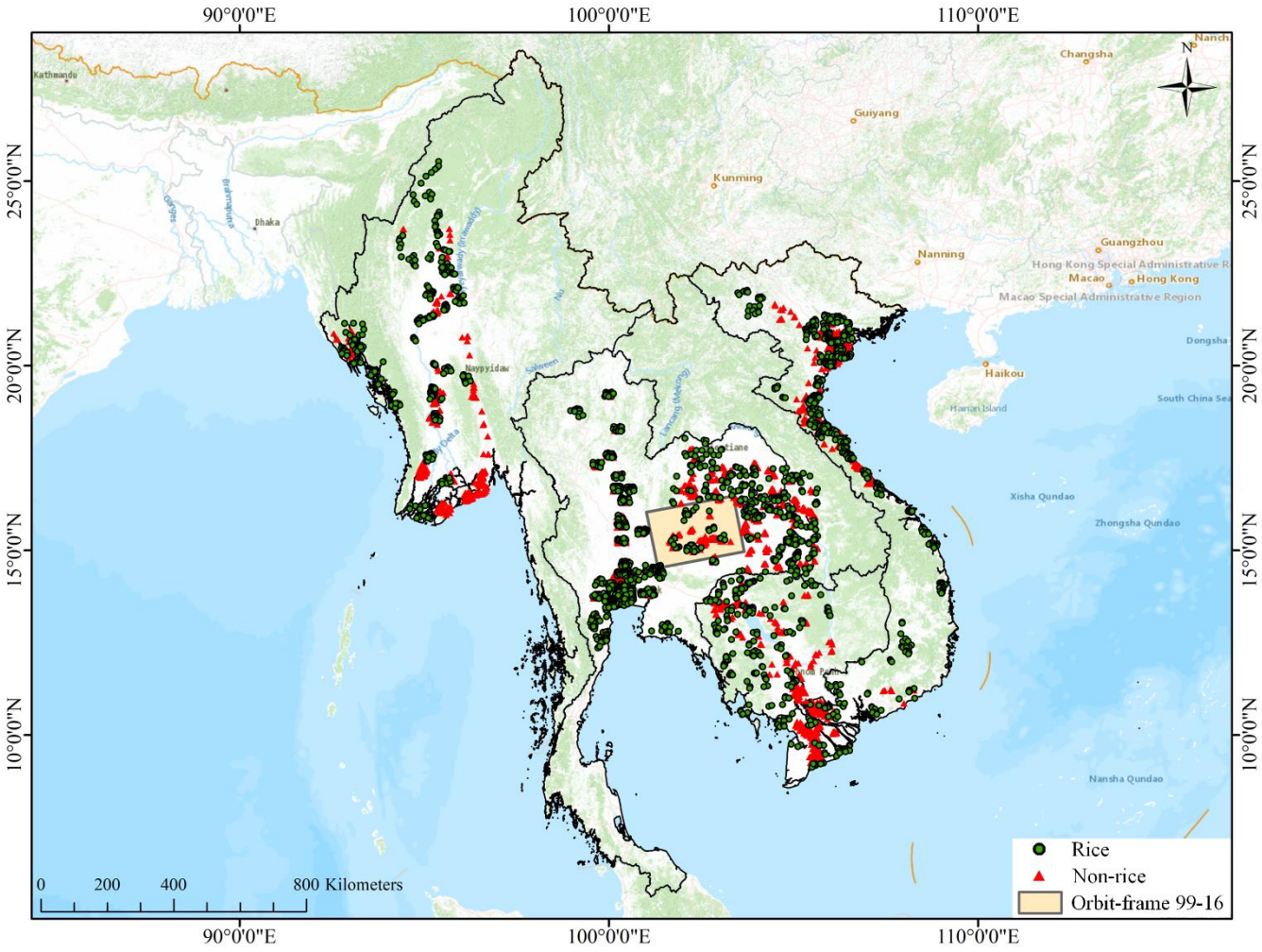


**Figure 1. Location of the study area. The Sentinel-1 data with Orbit-frame 99-16 were used for the training samples, and the Rice and Non-rice flags show the distribution of the validation sample set. The base map is from Esri.**

## 2.2 Data source

### 2.2.1 Satellite imagery and auxiliary data

The European Space Agency (ESA) provides a free data source for global land cover monitoring through Sentinel-1A, launched in 2014, and Sentinel-1B, launched in 2016 (Torres et al., 2012). The Sentinel-1 satellites carry a C-band (5.405 GHz) synthetic-aperture radar with a 12-day revisit period. In this study, the 2019 dual-polarized (VV/VH) GRD products in

Interferometric Wide Swath (IW) mode were downloaded from the ASF website. In total, 12 tracks, 90 frames and 2665 scenes of data were acquired. Details are shown in Table 1.

**Table 1. List of Sentinel-1 SAR data in 2019 used in this study**

| Country | Satellite | Orbit-Frame | Number of images | Country | Satellite | Orbit-Frame | Number of images | Country | Satellite | Orbit-Frame | Number of images |
|---|---|---|---|---|---|---|---|---|---|---|---|
| **Experimental Data** | | | | | | | | | | | |
| Myanmar | S1A | 41-44 | 31 | Thailand | S1B | 62-1 | 29 | Vietnam | S1A | 55-31 | 31 |
| | | 41-50 | 31 | | | 62-2 | 29 | | | 55-37 | 31 |
| | | 41-55 | 31 | | | 62-3 | 29 | | | 55-42 | 31 |
| | | 41-60 | 31 | | | 62-4 | 29 | | | 55-47 | 31 |
| | | 41-65 | 31 | | | 62-5 | 29 | | | 55-62 | 31 |
| | | 41-70 | 31 | | S1A | 62-20 | 27 | | | 55-67 | 31 |
| | S1A | 70-1217 | 31 | | | 62-21 | 27 | | | 55-72 | 31 |
| | | 70-1222 | 31 | | | 62-22 | 26 | Laos | S1A | 26-44 | 31 |
| | | 70-1227 | 31 | | | 62-23 | 24 | | | 26-49 | 31 |
| | | 70-1232 | 31 | | | 62-24 | 25 | | | 26-54 | 31 |
| | | 70-1237 | 31 | | S1B | 91-1 | 32 | | | 26-59 | 31 |
| | | 70-1242 | 31 | | | 91-2 | 32 | | | 26-64 | 31 |
| | | 70-1247 | 31 | | | 91-3 | 32 | | | 26-69 | 31 |
| | | 70-1252 | 31 | | | 91-4 | 32 | | S1A | 99-1240 | 30 |
| | | 70-1257 | 31 | | S1A | 135-16 | 23 | | | 99-1245 | 30 |
| | | 70-1262 | 31 | | | 135-17 | 23 | | | 99-1250 | 30 |
| | | 70-1267 | 31 | | | 135-18 | 23 | | S1A | 128-44 | 30 |
| | S1A | 143-46 | 30 | | | 135-19 | 23 | | | 128-49 | 30 |
| | | 143-51 | 30 | | S1B | 164-1 | 32 | | | 128-54 | 30 |
| | | 143-56 | 30 | | | 164-2 | 32 | | | 128-59 | 30 |
| | | 143-61 | 30 | | | 164-3 | 32 | | | 128-64 | 30 |
| | | 143-66 | 30 | | | 164-4 | 32 | Cambodia | S1A | 26-29 | 28 |
| | | 143-71 | 30 | | | 164-5 | 32 | | S1B | 26-32 | 30 |
| | | 143-76 | 30 | | S1A | 164-20 | 13 | | | 26-38 | 30 |
| | S1A | 172-1248 | 28 | | S1A | 172-17 | 31 | | | 26-43 | 30 |
| | | 172-1253 | 28 | | | 172-18 | 31 | | S1A | 99-1220 | 30 |
| | | 172-1258 | 28 | Vietnam | S1A | 26-23 | 28 | | | 99-1225 | 30 |
| | | 172-1263 | 28 | | | 26-34 | 31 | | S1B | 99-31 | 31 |
| | | 172-1268 | 28 | | S1A | 128-29 | 30 | | S1A | 128-34 | 30 |
| | | 172-1273 | 28 | | | 128-69 | 30 | | | 128-39 | 30 |
| **Training Dataset** | | | | | | | | | | | |
| Thailand | S1A | 99-16 | 29 | | | | | | | | |

And, the DEM and land use/land cover product were also collected. Shuttle Radar Topography Mission (SRTM) 3sec DEM product was used for terrain correction of SAR data. WorldCover data were used to reduce false alarms caused by water and woodland. WorldCover is a global land cover product produced by ESA and several scientific institutions using Sentinel-1 and Sentinel -2 data (Zanaga et al., 2021). It provides information on 11 land cover types for 2020 with a resolution of 10 m and an overall accuracy of 80.7% for the Asian region.

### 2.2.2 Agricultural statistics

The statistical yearbooks of each country were collected to compile annual census data of rice harvested area at different administrative levels in these countries. The administrative levels include national and subnational levels (state, province, or

regions, uniformly represented by province in this study). The unit of area in the statistical data is uniformly converted to hectares (ha).

### 2.2.3 Available rice maps based on remote sensing data

From the perspective of resolution and coverage area, 2 publicly downloadable rice maps were selected for comparison.

(1) Vietnam-wide annual land use/land cover datasets (VLUCD)

Researchers from the Japan Aerospace Exploration Agency (JAXA) produced the first 30-m resolution Vietnam-wide annual land use/land cover datasets (VLUCD) using multiple sources of data (including Landsat and Sentinel-1/2) and a random forest algorithm (Phan et al., 2021). The VLUCD contains annual land cover products for 1990-2020, including a primary classification (10 different categories of primary land cover, including rice) and a secondary classification (18 different categories of secondary primary land cover, including rice). The rice layer was extracted from the 2019 annual land cover products for comparison.

(3) Rice data of Asia from International Rice Research Institute (IRRI Rice Data)

The International Rice Research Institute (IRRI) is an international agricultural research and training organization with its headquarters in Los Baños, Laguna, in the Philippines, and offices in seventeen countries. IRRI is one of 15 agricultural research centers in the world that form the Consortium of International Agricultural Research Centers(CGIAR), a global partnership of organizations engaged in research on food security. IRRI is also the largest non-profit agricultural research center in Asia. The IRRI produced a 500 m resolution map of the general distribution of rice in Asia from 2001 to 2012 using MODIS time-series data (Nelson and Gumma, 2015), which is freely available to the public.

Table 2 shows details of the SAR data, auxiliary data, available rice maps, land cover data and statistics used in the study.

**Table 2. Data information used in the study**

| Data type | Data product or country name | Year | Resolution | Description of use | Data access | Last access (dd/mm/yyyy) |
|---|---|---|---|---|---|---|
| SAR imagery | Sentinel-1 | 2019 | 20*22 m (rg*az) | The backscatter characteristics extraction | https://search.asf.alaska.edu/#/ | 11/10/2022 |
| DEM | Shuttle Radar Topography Mission (SRTM) 3sec | 2000 | 90m | Terrain correction | https://search.earthdata.nasa.gov/search?q=SRTM | 11/10/2022 |
| Land cover data | ESA WorldCover 2020 | 2020 | 10 m | Generation of water and woodland masks | https://esa-worldcover.org/en | 11/10/2022 |
| Available rice area map | Vietnam-wide annual land use/land cover datasets (VLUCD) | 2019 | 30 m | Spatial consistency assessment | https://www.eorc.jaxa.jp/ALOS/en/dataset/lulc/lulc_vnm_v2109_e.htm | 11/10/2022 |
| | Rice data of Asia from IRRI (IRRI Rice Data) | 2000 to 2012 | 500 m | Spatial consistency assessment | https://www.irri.org/mapping | 11/10/2022 |
| Statistical yearbook | Vietnam | 2019 | Province scale | Precision verification | https://www.gso.gov.vn/en/homepage/ | 11/10/2022 |
| | Cambodia | 2019 | Province scale | Precision verification | http://nis.gov.kh/index.php/km/ | 11/10/2022 |
| | Laos | 2019 | Province scale | Precision verification | https://www.lsb.gov.la/en/home/ | 11/10/2022 |
| | Thailand | 2019 | Province scale | Precision verification | http://www.nso.go.th/sites/2014en | 11/10/2022 |
| | Myanmar | 2019 | State scale | Precision verification | https://www.mopf.gov.mm/en/page/planning/central-statistical-organization-cso/752 | 11/10/2022 |

## 3 Method

The flowchart of this study is shown in Figure 2. First, the Sentinel-1 time series images were preprocessed. Then, key features in the rice growth process are extracted from the time series SAR data. To make full use of the pixel-level semantics of the features, the extracted features were fed into the U-Net model to obtain rice area extraction results with spatial details. Finally, to reduce false alarms from water bodies and non-rice vegetation, the results were postprocessed using masks generated based on high-precision land cover products to obtain the annual rice area map of five Southeast Asian countries.

### 3.1 Preprocessing

The Sentinle-1 time-series data were preprocessed using the Sentinel Application Platform (SNAP) software (Filipponi, 2019). The SNAP is a common architecture for all Sentinel Toolboxes. ESA/ESRIN is providing the SNAP user tool free of charge to the Earth Observation Community.

The steps were as follows: (1) Orbit correction: This operation refines the inaccurate orbit state vectors provided in the metadata of a SAR product with the precise orbit files which are available days to weeks after the generation of the product;(2) Thermal noise removal: Because SAR are contaminated by additive thermal noise, this step is introduced to mitigate thermal noise effects;(3) Radiometric calibration: This process provides the image in which the pixel values can be directly related to the radar backscatter of the image;(4) Coregistration: This step co-registers multitemporal intensity images; (5) Terrain correction: This process converts SAR data from the slant or ground range projection to geographic coordinate projection and corrects the distortion effects that occurred during the acquisition (overlay, shading);(6) Multitemporal speckle noise filtering: This operation reduces speckles, which degrade the quality of the image and make interpretation of features more difficult;(7) Converting values to decibels: This step convers the multitemporal intensity map to sigma 0 ($\sigma^0$) on the decibel (dB) scale using a logarithmic transformation. The final $\sigma^0$ images with 20 m resolution in the WGS84 geographic coordinate system were obtained.

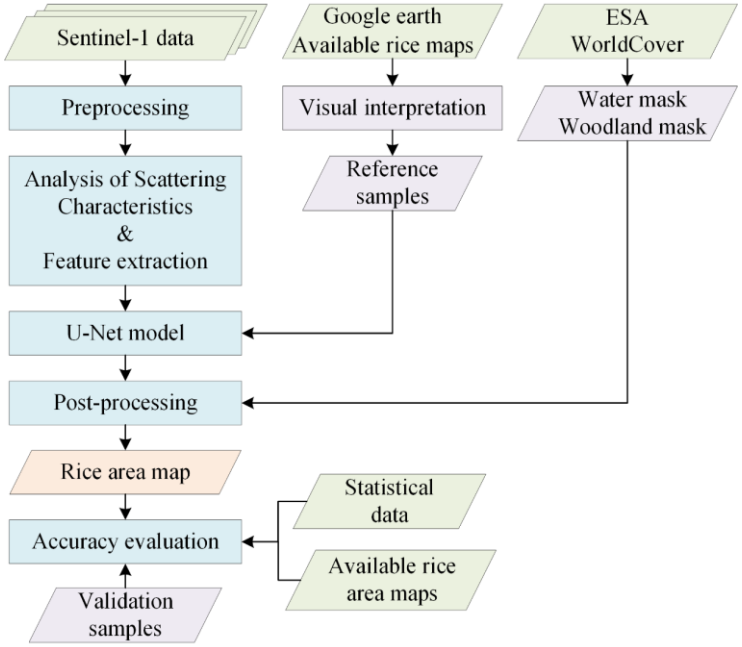


**Figure 2. Flowchart of the proposed rice area mapping method using Sentinel-1 data.**

### 3.2 Feature Extraction

As described in many previous studies (Singha et al., 2019; Chang et al., 2020; Crisóstomo De Castro Filho et al., 2020; Sun et al., 2022a), VH polarization was more sensitive to the flooding period of rice than VV polarization and has been more widely used for rice area extraction. Therefore, Sentinel-1 VH polarization time series data were selected in this study. To analyze the timeseries characteristics of the backscattering coefficients of rice and other land cover types in the study area, representative sample plots of four typical land cover types (rice, water bodies, buildings, and non-rice vegetation) were

selected. Based on Google Earth data and other land cover data, four rice regions that belongs to different cropping systems were chosen. The average VH polarization time series data of these land cover types were calculated, as shown in Figure 3.

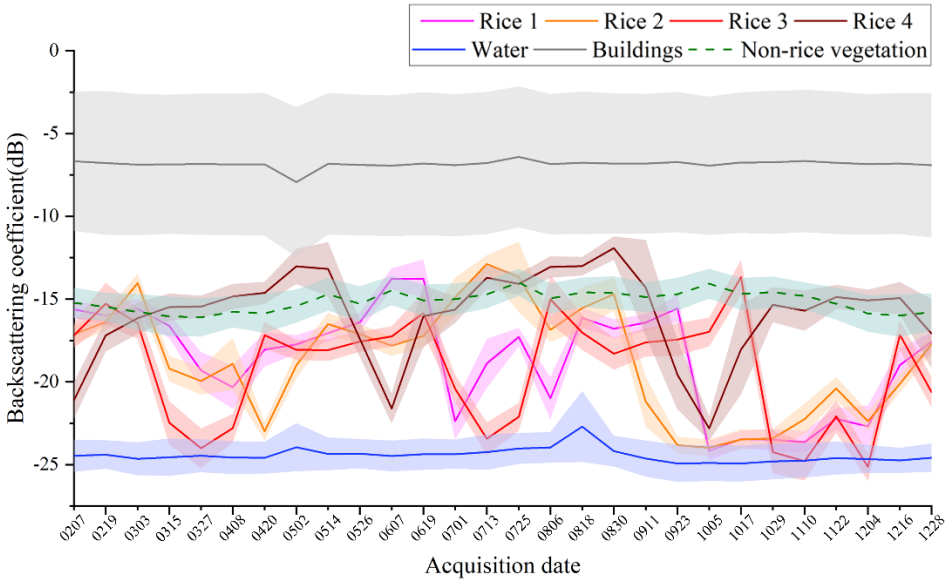


**Figure 3. The average VH polarization backscattering coefficient curve of typical landcovers (The shaded areas refer to the standard deviation calculated from the sample points).**

In Figure 3, the backscattering coefficients of water bodies were small, as they exhibited single specular scattering, and their return power was lower than that of other land covers. In contrast, buildings exhibited double bounce and their return powers were much stronger, leading to larger backscattering coefficients. The scattering process of radar waves of non-rice vegetation was more complicated, and the backscattering coefficients of non-rice vegetation were between buildings and water bodies. For different kinds of rice samples, the curve fluctuations were significant, due to the effects of flooding and multi-season planting patterns. But generally, their backscattering intensities ranged between buildings and water bodies.

More specifically, during the observation period, two seasons of rice were planted in the land parcel of Rice 1, the first from April to July and the second season from August to October. The land parcel of Rice 2 was planted with only one season of rice, from April to September. The land parcel of Rice 3 was planted with two seasons of rice: the first season was from March to July and the second season was from July to October. The land parcel of Rice 4 was planted with three seasons of rice: the first season was from February to June, the second season was from June to October, and only part of the third season (October-December) was observed. It can be seen that the time steps of each growing season for the selected Rice 1- Rice 4 were inconsistent. In fact, the high heterogeneity of rice backscattering coefficients in Southeast Asia is caused by the high heterogeneity in climate and topography. This makes the backscatter coefficient curves of the rice growth cycle more diverse and does not allow us to summarize a generalized model of rice evolution. Therefore, it will be difficult to accomplish the rice field extraction task using a direct reliance on the fixed relationship between phenology and time.

Through a large number of comparative experimental analysis and combined with our previous research work (Xu et al., 2022), three time-series statistical features that can describe the most significant SAR characteristics during rice growth were selected for rice area mapping in the study area, namely, the sharpness of the change in $\sigma^0$ ($\sigma^0_{var}$), the minimum value of the backscatter coefficients in the time-series ($\sigma^0_{min}$), the maximum value of backscatter coefficients in the time-series ($\sigma^0_{max}$).

The interaction between the crop canopy and microwave radiation varies with time during plant growth. In contrast, the backscattering coefficients of non-crops, such as water bodies, buildings and woodland, are more stable. Therefore, the sharpness of the change in $\sigma^0$ with time will be a key factor in distinguishing cropland from other land cover types. $\sigma^0_{var}$ is given by the following equation.

$$\sigma^0_{var} = \frac{1}{n}\sum_i^n \left|\sigma^0_i - \sigma^0_{mean}\right|^2 \quad (1)$$

where $\sigma^0_{mean} = \frac{1}{n}\sum_i^n \sigma^0_i$, $n$ is the number of images.

During the flooding stage, the backscattering characteristics of rice are significantly different from other crops that do not require extensive irrigation, and are close to that of water. Therefore, this study identified the flooding stage by calculating the minimum value of the backscatter coefficient in the time-series images to distinguish rice from other crops. $\sigma^0_{min}$ is given by Equation (2).

$$\sigma^0_{min} = min\{\sigma^0_1, \sigma^0_{2,}\sigma^0_3, \dots, \sigma^0_n\} \quad (2)$$

The seasonal backscattering variation exhibited by water bodies can interfere with the identification of rice. In contrast to the seasonal variation of water bodies, the backscatter coefficient of rice shows a substantial increase during the growth process. Therefore, false alarms generated by water bodies can be reduced by identifying the maximum value of backscatter coefficients in the time-series images. $\sigma^0_{max}$ is given by the following equation.

$$\sigma^0_{max} = max\{\sigma^0_1, \sigma^0_{2,}\sigma^0_3, \dots, \sigma^0_n\} \quad (3)$$

A pseudo-color image is synthesized in the order of R: $\sigma^0_{max}$, G: $\sigma^0_{min}$, and B: $\sigma^0_{var}$,shown in Figure 4. Due to the higher $\sigma^0_{var}$ and $\sigma^0_{max}$ and lower $\sigma^0_{min}$ of rice, the color of rice in the pseudo-color composite image is mainly purplish red, sometimes red or dark blue. Compared to other land covers, water bodies have lower $\sigma^0_{var}$, $\sigma^0_{max}$ and $\sigma^0_{min}$. Therefore, water bodies are black in the pseudo-color image. Land covers with less variation in backscatter intensity, such as settlement and non-rice vegetation, generally have smaller $\sigma^0_{var}$and higher $\sigma^0_{min}$. Therefore, the colors of these land covers are usually yellow or green in the pseudo-color image.

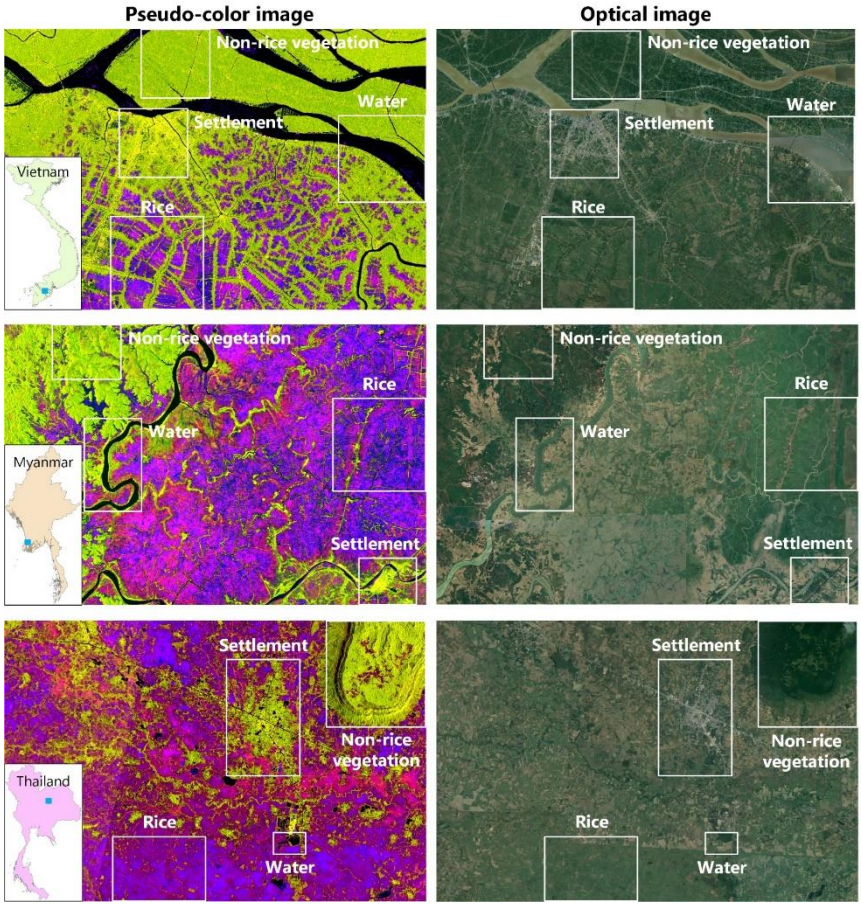


**Figure 4. The pseudo-color image synthesized from three SAR feature parameters (R: $\sigma^0_{max}$; G: $\sigma^0_{min}$; B: $\sigma^0_{var}$) and the corresponding optical image from Google Earth ©Google Earth.**

### 3.3 Training and validation sets

The above analysis shows that, the rice and non-rice landcovers of these Southeast Asian countries have consistent features in the pseudo-color image, i.e. the model trained by one scene was applicable for all other scenes with good transferability. Therefore, a training dataset generated from the orbit-frame 99-16 images of Thailand from previous work (Xu et al., 2021) was used, as shown in Figure 1. A sliding window with a pixel size of 224×224 was used to slice the training images into image patches with 50% overlap. The training dataset consisted of 15659 image patches with a pixel size of 224×224. A validation sample set for accuracy evaluation was collected using auxiliary data such as Google Earth optical images and other rice maps. The validation samples were divided into two categories, rice and non-rice, the number of samples is shown in Table 3 and their distribution is shown in Figure 1.

**Table 3. Information of validation sample set**

| Class | Number of plots | Number of pixels |
|---|---|---|
| Rice | 1913 | 2,128,431 |
| Non-rice | 2032 | 2,188,477 |

### 3.4 U-Net Model

In this paper， high-precision rice area mapping was accomplished using U-Net model. U-Net is a classical semantic segmentation model widely used in biomedical image segmentation and remote sensing (Wei et al., 2019; Xu et al., 2021; Lin et al., 2022). It outputs semantically labeled pixel-by-pixel images corresponding to the input image while extracting high-level semantic features, so that the spatial details of the input image can be maintained (Ronneberger et al., 2015). A SAR image covers a large spatial area, which include multiple ground objects with complex and rich semantic information; rice fields are spatially characterized by continuous and large distribution. Therefore, U-Net is used to fully combine the spatial and semantic information in SAR images to achieve high-precision rice area extraction.

The structure of U-Net model is shown in Figure 5. U-Net consists of encoder (contracting path) and decoder (expansive path). The encoder is used for feature extraction, and the decoder is used to restore the size of the input image. U-Net has 23 convolutional layers, including eighteen 3×3 convolutional layers, four 2×2 convolutional layers and one 1×1 convolutional layer. The encoder part consists of five downsampling units, where each unit consists of two 3×3 convolutional layers and a 2×2 max-pool layer. The output of the downsampling unit is input to the next downsampling unit by max-pooling. The decoder contains four upsampling units, each of which consists of two 3×3 convolutional layers and a 2×2 deconvolutional layer. In the final stage of the decoder, the feature vector of the last upsampling unit is converted into a probability mapping by the 1×1 convolutional layer. The dimension of the probability mapping is 2 and the pixel value indicates the probability that the pixel belongs to rice and non-rice.

Meanwhile, thanks to the U-shaped structure and skip connection, each downsampling is cascaded with the corresponding upsampling, and this fusion of features at different scales is greatly helpful for upsampling to recover pixels. Specifically, the shallow downsampling multiplier is small and the feature map has more detailed rice spatial distribution features (low-level spatial features). While the deep downsampling multiplier is large and the information is heavily condensed with large spatial loss. But the high-level semantic features obtained from deep downsampling help in the determination of rice regions. When the high-level and low-level features are fused, it helps to improve the segmentation accuracy.

To solve the problem of uneven data distribution, we added a batch normalization (BN) layer (Ioffe and Szegedy, 2015) before each convolutional layer. The BN layer allows the input data to follow the same distribution to achieve regularization of the model.

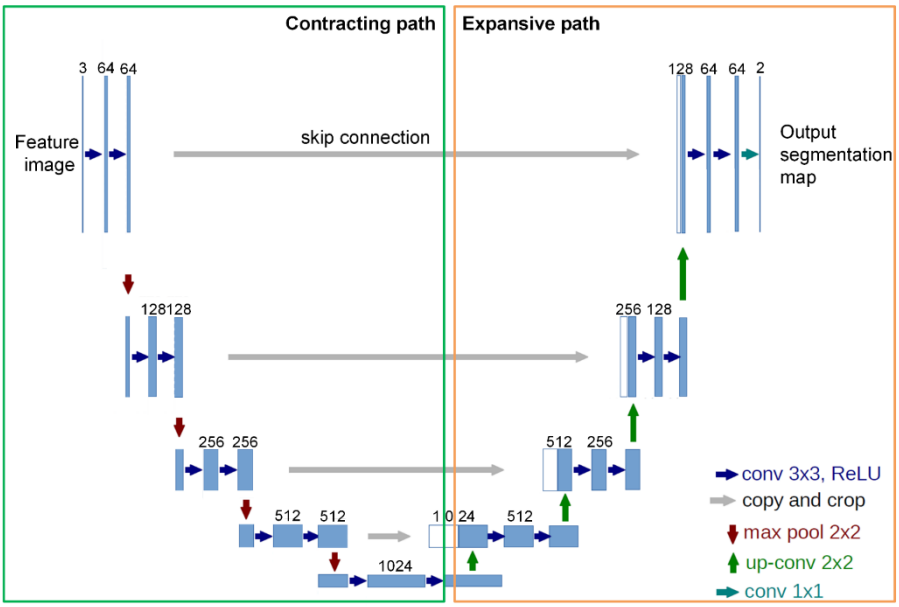


**Figure 5. Structure of the U-Net model.**

### 3.5 Postprocessing

In rice area mapping, water bodies (e.g., rivers and lakes) can confuse the flooding signal of rice. In addition, non-rice vegetation may cause some disturbances due to weather effects.

Therefore, as drawn on many studies (Cué La Rosa et al., 2019; Sun et al., 2021), water body masks and woodland masks produced by WorldCover were used to reduce false alarms of rice field extraction results to some extent.

### 3.6 Accuracy evaluation

In this study, several strategies were used to evaluate our rice map product, including accuracy assessments based on validation sets and comparisons with statistical data and other rice maps at the national and provincial levels. First, common accuracy metrics based on the validation set were calculated to measure the classification effectiveness of the model, including accuracy, precision, recall, and kappa (Congalton, 1991; Vapnik, 1999; Mchugh, 2012).

$$Accuracy = \frac{TP + TN}{TP + TN + FN + FP} \tag{4}$$

$$Precision = \frac{TP}{TP + FP} \tag{5}$$

$$Recall = \frac{TP}{TP + FN} \tag{6}$$

$$Kappa = \frac{accuracy - P_e}{1 - P_e} \tag{7}$$

$$P_e = \frac{(TP + FP) \times (TP + FN) + (FN + TN) \times (FP + TN)}{(TP + TN + FN + FP)^2} \quad (8)$$

where *TP* denotes the number of pixels correctly classified as rice, *TN* denotes the number of pixels correctly classified as non-rice, *FP* denotes the number of pixels misclassified as rice among non-rice pixels, *FN* denotes the number of pixels misclassified as non-rice among rice pixels, and *P*e is the desired accuracy.

Second, the spatial consistency of rice field extraction results with statistical data and other rice maps was compared at the national and provincial levels. The coefficient of determination ($R^2$) of the rice area map with statistical data and other rice area maps was calculated using the following equation (Draper and Smith, 1998).

$$R^2 = \frac{\left(\sum_{i=1}^{n}(x_i - \bar{x}_i) \times (k_i - \bar{k}_i)\right)^2}{\sum_{i=1}^{n}(x_i - \bar{x}_i)^2 \times \sum_{i=1}^{n}(k_i - \bar{k}_i)^2} \quad (9)$$

where $n$ is the total number of administrative units, $x_i$ is the area of extracted rice, $\bar{x}_i$ is its corresponding mean value, $k_i$ is the area of statistical data or other rice maps and $\bar{k}_i$ is its corresponding mean value.

## 4 Results

The 2019 rice area map for mainland Southeast Asia using Sentinel-1 SAR data was shown in Figure 6. According to the extraction result, the main rice production areas in Myanmar are located in the Ayeyarwady, Bago and Yangon delta regions, which are crossed by river systems. In addition, Mandalay, Sagaing and Magwayue in the northern arid mountainous region also play an important role in rice production. Thailand's rice fields are concentrated in the central plains, north and northeast. The main rice-producing areas in Laos are located in the central and southern lowland areas. Many of the major rice-producing provinces are located along the Mekong River, such as Borikhamxay, Khammouane, Savannakhet, Salavan, and Champasak. Rice fields in Cambodia are concentrated in the Tonle Sap Lake basin and the southern Mekong River basin. In Vietnam, the representative rice planting areas are the Mekong Delta and the Red River Delta.

Next, the rice area map was evaluated as comprehensive as possible from three different scales. First, the validation sample set introduced in the previous section was used to evaluate the accuracy of rice area mapping from the methodological level. Second, at the national level, the rice area maps were compared with statistical data on rice harvested area and other available rice area maps, respectively. Finally, at the provincial level, more detailed comparisons were made with statistical data and other provincial rice area maps to measure the spatial consistency between the extracted rice distribution and these data.

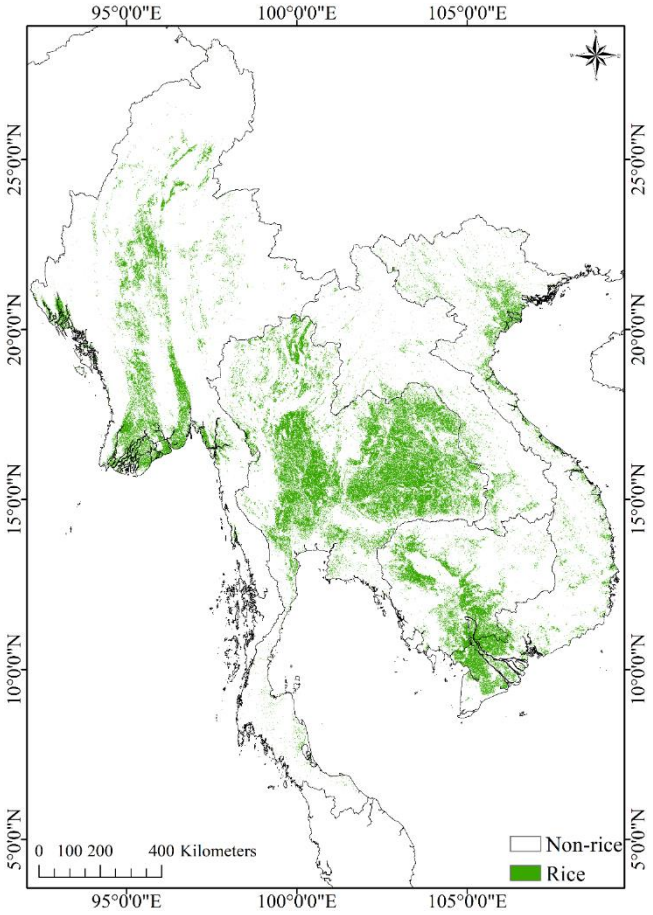


**Figure 6. 20m resolution rice area map of five countries in mainland Southeast Asia in 2019.**

### 4.1 Accuracy based on the validation set

The accuracies of the rice area map based on the validation sample set is shown in Table 4. Among them, the accuracy was as high as 92.20%, and the Kappa was 0.8425, which proved that the proposed method had good classification performance. The precision was 92.45%, indicating that the method could effectively reduce the false alarms in the rice area extraction results. Therefore, these precision metrics illustrated that the rice mapping results were in good agreement with the validation samples. It also further demonstrated the capability of the proposed method for rice area mapping in large tropical regions.

**Table 4. Accuracy of the rice area map based on the validation set**

| Class | Accuracy | Precision | Recall | Kappa |
|---|---|---|---|---|
| Rice | 92.20% | 92.45% | 90.26% | 0.8425 |

### 4.2 Comparison with statistical data and other rice area maps at the national scale

Figure 7 showed the comparison of the extracted rice area with statistical data and the IRRI rice data at the national level scale for five Southeast Asian countries. As seen from the figure, the extraction results were consistent with both statistical data and IRRI rice data. Most points were distributed in the vicinity of the 1:1 line. In contrast, the extraction result was better consistent with IRRI, $R^2$ can reach 0.93, while $R^2$ with statistical data was 0.78.

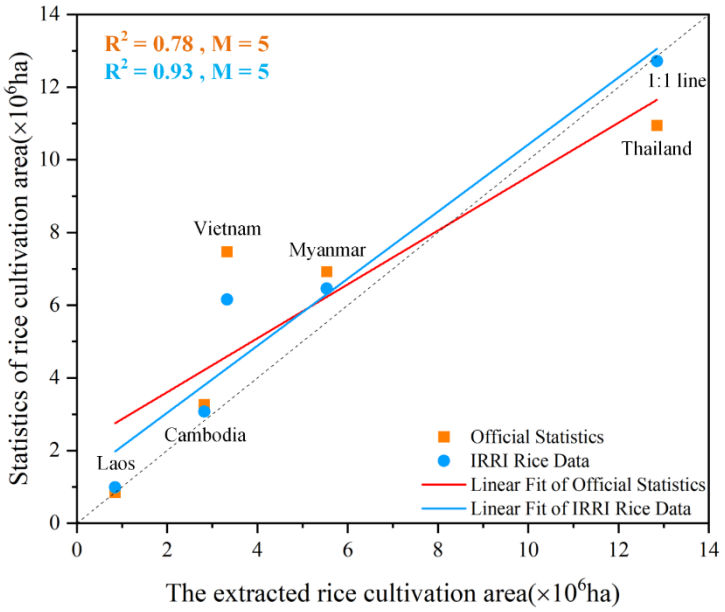


**Figure 7. Comparison of the extracted rice area with statistical rice harvested area and IRRI dataset at national level scale. M is the number of countries.**

**Table 5. Statistics, other rice area maps and the extracted rice area for five Southeast Asian countries.**

| Country | Statistics of rice cultivation area ($\times 10^{-6}$ ha) | IRRI rice data ($\times 10^{-6}$ ha) | Statistics of paddy land area ($\times 10^{-6}$ ha) | VLUCD ($\times 10^{-6}$ ha) | Extracted rice cultivation area ($\times 10^{-6}$ ha) |
|---|---|---|---|---|---|
| Thailand | 10.9442 | 12.7198 | - | - | 12.8508 |
| Cambodia | 3.2638 | 3.0740 | - | - | 2.8215 |
| Myanmar | 6.9209 | 6.4575 | - | - | 5.5390 |
| Laos | 0.8435 | 0.9856 | - | - | 0.8458 |
| Vietnam | 7.4695 | 6.1527 | 4.1205 | 3.8210 | 3.3270 |

Table 5 showed the statistical area of rice, the area of other rice area maps and the area of rice extraction for five Southeast Asian countries. As shown in Figure 7 and Table 5, compared with IRRI rice data, the extraction area of Cambodia, Laos and Thailand was close to that of IRRI, while that of Myanmar and Vietnam was slight lower. Compared with the statistical data, the extraction areas of Cambodia and Laos were in good agreement with the statistical data. The extraction area of rice in Myanmar and Vietnam was lower, while that in Thailand was slightly higher.

It could be seen that the statistics of rice harvested area were much higher than the area of rice extracted of Vietnam. The statistical data were the total rice harvest areas in different growing seasons each year, but the extracted rice area was the land area where rice was planted. In Vietnam, there are three seasons of rice, namely, spring rice, autumn rice and winter rice, while the harvested areas of spring rice and autumn rice are comparable, and the harvested area of winter rice is smaller. In this way, part of the statistical data of rice harvest area is repeated and accounts for a large proportion of the area, resulting in a larger rice statistical area than the extracted rice area. Although other countries also have multiple rice seasons, the areas of rice in the main season are large, while that in other seasons is small, so the area proportion calculated repeatedly is small. The extracted rice area was closer to the paddy land area in statistical yearbook of Vietnam and VLUCD, indicating that the extraction result was reliable.

### 4.3 Comparison with statistical data and other rice maps at the provincial scale

Figure 8 shows the comparison of the extracted rice area with the statistical data of rice harvested area and IRRI rice data at the provincial scale for five Southeast Asian countries. The available rice maps contain a 500 m resolution rice map of mainland Southeast Asia (IRRI Rice Data) and a 30 m resolution rice map of Vietnam (VLUCD) (see Sect. 2.2.3 for details). In general, the rice area extraction results were in good agreement with the statistical area, IRRI data and VLUCD. Among them, the $R^2$ ranged from 0.82 to 0.88 with statistical data and from 0.83 to 0.97 with IRRI, as shown in Figure 8.

As shown in Figure 8 (a) and (b), the rice planting areas in Thailand and Cambodia extracted by our method had a good correlation with the statistical data and IRRI data at the provincial scale. The $R^2$ was distributed in the range of 0.83-0.88. There were no provinces with large deviations.

In Figure 8(c), in Myanmar, the $R^2$ between the extracted area of rice and the statistical data, IRRI rice data was 0.83 and 0.84, respectively. However, the extracted rice area of Ayeyarwady Province was significantly lower than that of the statistical data and IRRI data. The extraction results of Ayeyarwady were compared with the IRRI data, as shown in Figure 9. As reported by Han et al. (Han et al., 2021), due to the influence of mixed pixels, the IRRI data divides too many rivers and non-rice vegetation into rice. And the extracted rice map retains the details of rivers and roads.

The $R^2$ of the extracted rice area in Laos with statistical data was 0.82, and the highest agreement with IRRI data was 0.97, as shown in Figure 8(d). For the same reason as Ayeyarwady Province, the rice extraction area in Savannakhet Province was lower than the IRRI data because the details of rivers and roads were preserved in the extraction results.

Different from other sub figures, Vietnam added data comparison results with 30m VLUCD. The extraction results in Vietnam correlated well with the statistical data, VLUCD and IRRI data, with all $R^2$ values greater than 0.80, as shown in Figure 8(e). The area of rice extraction in Vietnam was in higher agreement with VLUCD ($R^2$ of 0.87) than with statistics ($R^2$ of 0.86) and IRRI Rice Data ($R^2$ of 0.83). Most of the points of VLUCD were distributed on the 1:1 line.

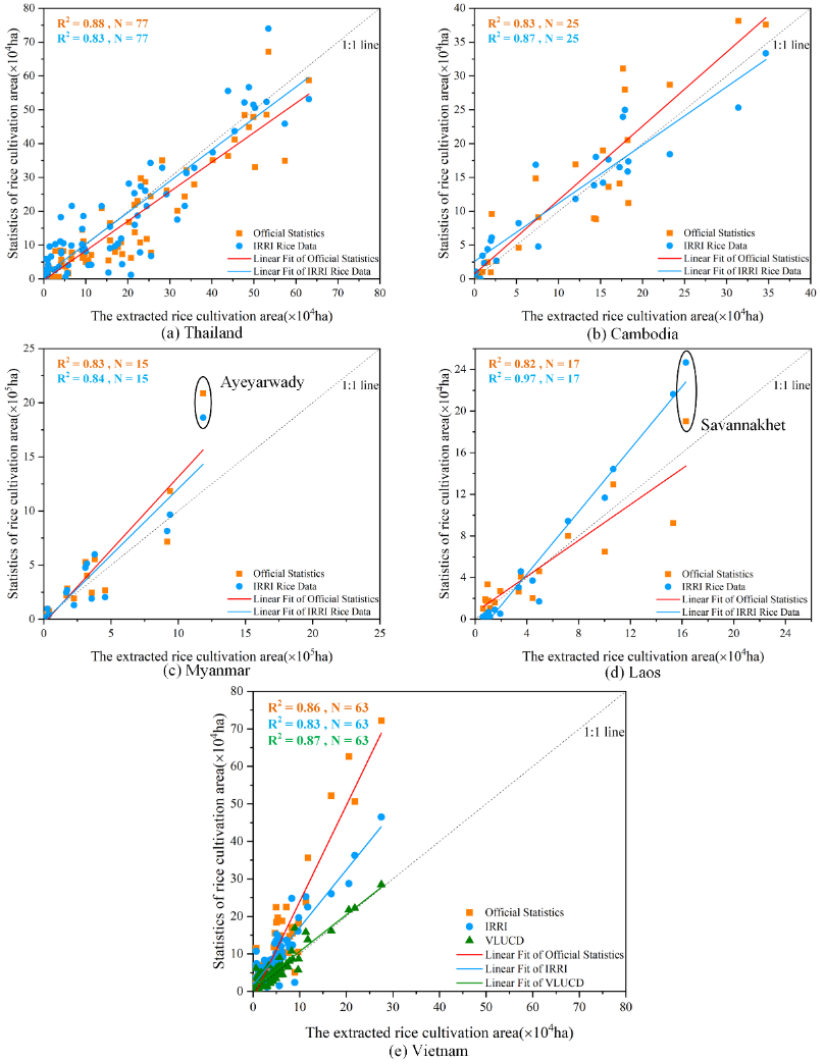


380 **Figure 8. Comparison of the extracted rice area with statistical rice harvested area and IRRI dataset at provincial scale. N is the number of provinces in each country.**

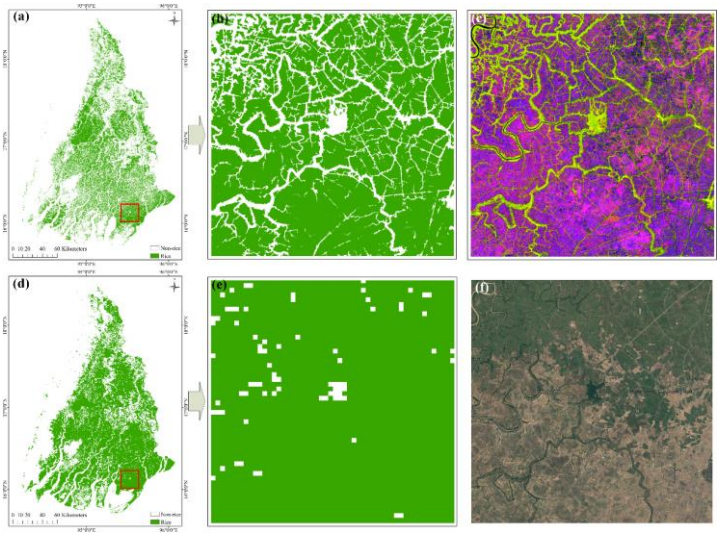

**Figure 9**. Comparison of our extracted rice area map of Ayeyarwady Province with IRRI data: (a) our rice area extraction result; (b) the enlarged view of the red box in (a); (c) the pseudo-color image of SAR features corresponding to (b); (d) RRI rice data; (e) the enlarged view of the red box in (d); (f) the Google Earth optical image © Google Earth corresponding to(e).

## 5 Discussion

In this study, annual rice area maps for five Southeast Asian countries in 2019 were generated using temporal features extracted based on Sentinel-1SAR time series and an improved U-Net model. Accuracy, Precision, and Recall based on the validation set exceeded 90% with a Kappa of 0.8425. Accuracy evaluation of rice mapping showed that the proposed temporal features were able to portray the unique growth characteristics of rice, and the improved U-Net model was able to suppress the false alarms of sporadic distribution caused by complex topography. The proposed method has superior capability in mapping rice distribution in large tropical regions.

The rice area extraction results were compared with statistical data from the national and provincial levels in Sections 4.2 and 4.3. The results of multiple comparisons show that our rice area extraction results are in high agreement with the statistical data. However, there were also minor inconsistencies. A possible reason is that the statistical cycle is not strictly aligned with the SAR data collection cycle. The rice area extracted in this study is the total area of all fields that have been planted with rice in a year. Most agricultural statistics record the total area of rice planted in different growing seasons on an annual basis or even from one month of one year to the next. In addition, the statistical methods may cause errors in the statistics. The well-organized rice growing seasons were mainly considered in all statistics, and the random and irregular planting behavior of individual farmers was inevitably ignored. Considering the data collection conditions and statistical errors, it is understandable that the extracted rice maps differ from the official statistics.

The comparison results between rice area products extracted based on different remote sensing data showed that our rice area extraction results were in good agreement with the available rice products at the national and provincial levels. To fully demonstrate the reliability of the rice extraction results, three subregions from the rice map were selected for comparison in Thailand and Vietnam, as shown in Figure 10. As mentioned in other literature (Dong et al., 2015; Han et al., 2021), the MODIS-based IRRI rice map with 500 m resolution contains a large number of mixed image elements, and thus misclassification exists in rice area maps. The spatial distribution characteristics of our rice area map were generally consistent with those of the IRRI data, and our rice map retained more details with fewer mixed pixels. In addition, our rice map also had better agreement with the spatial distribution and detailed information of rice from VLUCD. Overall, comparisons based on the validation set, statistical data, and other rice area map products confirmed the reliability of our rice area map.

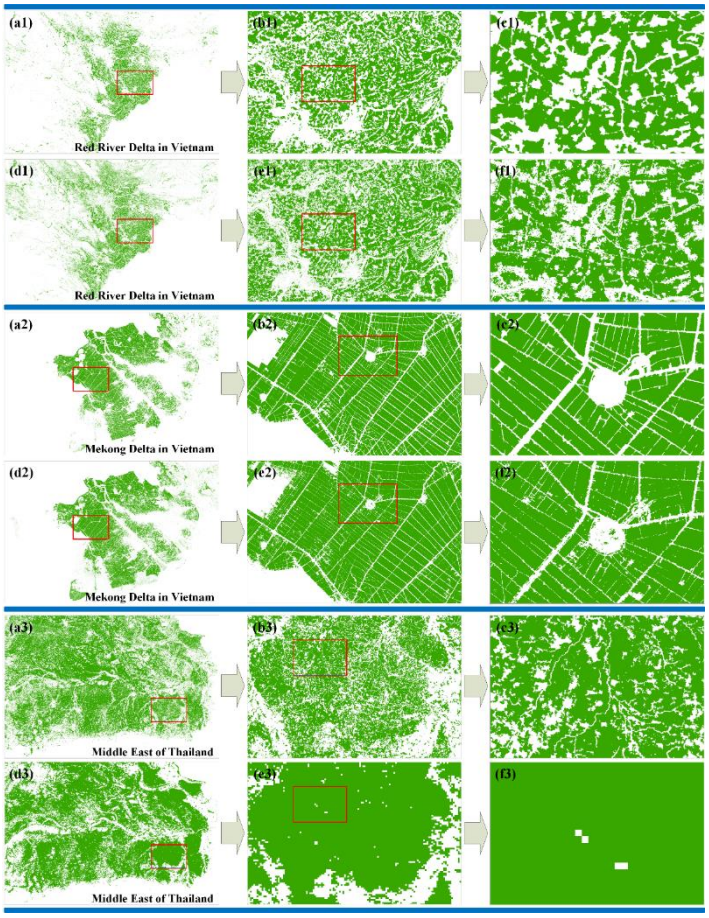


**Figure 10. Comparison of our rice area map with available rice area products in typical regions. Our extraction results (a1-c1, a2-c2, a3-c3); VLUCD rice map (d1-f1, d2-f2); IRRI rice data (d3-f3). The figures in the second column show the enlarged views of the red boxes in the figures of the first column, and the figures in the third column show the enlarged views of the red boxes in the figures of the second column.**

In the study, it is that the temporal features along rivers and wetlands are more similar to paddy rice and have similar colors in the feature pseudo-color image, which can be easily misclassified as rice. The backscattered information of scattered rice fields is subject to interference from topography and surrounding non-rice land cover, resulting in missed detection. Improvements can be made in future studies using water masks extracted from higher precision land cover data or by adding more negative samples.

## 6 Data Availability

The 20 m annual paddy rice area map for mainland Southeast Asia can be accessed at Zenodo dataset from the following DOI: https://doi.org/10.5281/zenodo.7315076(Sun et al., 2022b). The spatial reference system of the dataset is EPSG:4326(WGS84).

## 7 Conclusions

Ending hunger and malnutrition is essential, and rice plays a critical role. Satellite-based remote sensing offers the most practical means of monitoring rice cultivation in mainland Southeast Asia. Questions remain, however, as to appropriate timing, number of satellite observations, spatial resolution of satellite imagery, and effective data processing methods for rice distribution and production information.

To perform large-scale rice area mapping in tropical and subtropical regions, an efficient rice area mapping method based on time series SAR features and a deep learning model is proposed. A 20-meter spatial resolution rice area map of mainland Southeast Asia was produced using the 2019 Sentinel-1 time series data and the proposed rice area mapping method. The accuracy of the proposed method on the validation sample set was 92.20%. Our rice area maps correlated significantly with statistical data and were consistent with other rice area maps. These results demonstrate the advantages of the proposed method for rice area mapping with complex cropping patterns. The rice area maps we produced will provide data support for agricultural resource studies, such as yield prediction and agricultural management.

**Author Contributions:** Conceptualization, methodology, software, C.S. and H.Z.; validation, formal analysis, H.Z.; investigation, C.S. and L.X.; resources, data curation, J.J. and J.G.; writing—original draft preparation, C.S. and H.Z.; writing—review and editing, H.Z., L.X., J.G. and L.Z.; visualization, L.X. and J.G.; supervision, project administration, H.Z. and C.W. All authors have read and agreed to the published version of the manuscript.

**Funding:** This research was funded by the National Natural Science Foundation of China under Grants 41971395, 41930110 and 42001278 and the Strategic Priority Research Program of Chinese Academy of Sciences (XDA19090119).

**Acknowledgments:** The authors would like to thank ESA and EU Copernicus Program for providing the Sentinel-1 SAR data.

**Conflicts of Interest:** The authors declare no conflict of interest.

## References


Bridhikitti, A. and Overcamp, T. J.: Estimation of Southeast Asian rice paddy areas with different ecosystems from moderate-resolution satellite imagery, Agriculture, Ecosystems & Environment, 146, 113-120, https://doi.org/10.1016/j.agee.2011.10.016, 2012.

Chang, L., Chen, Y.-T., Chan, Y.-L., and Wu, M.-C.: A Novel Feature for Detection of Rice Field Distribution Using Time Series SAR Data, IGARSS 2020 - 2020 IEEE International Geoscience and Remote Sensing Symposium, 10.1109/igarss39084.2020.9323278, 2020.

Chen, C. F., Son, N. T., and Chang, L. Y.: Monitoring of rice cropping intensity in the upper Mekong Delta, Vietnam using time-series MODIS data, Advances in Space Research, 49, 292-301, 10.1016/j.asr.2011.09.011, 2012.

Chen, C. F., Son, N. T., Chen, C. R., Chang, L. Y., and Chiang, S. H.: Rice Crop Mapping Using Sentinel-1a Phenological Metrics, ISPRS - International Archives of the Photogrammetry, Remote Sensing and Spatial Information Sciences, XLI-B8, 863-865, 10.5194/isprsarchives-XLI-B8-863-2016, 2016.

Clauss, K., Yan, H., and Kuenzer, C.: Mapping Paddy Rice in China in 2002, 2005, 2010 and 2014 with MODIS Time Series, Remote Sensing, 8, 10.3390/rs8050434, 2016.

Clauss, K., Ottinger, M., Leinenkugel, P., and Kuenzer, C.: Estimating rice production in the Mekong Delta, Vietnam, utilizing time series of Sentinel-1 SAR data, International Journal of Applied Earth Observation and Geoinformation, 73, 574-585, 10.1016/j.jag.2018.07.022, 2018.

Congalton, R. G.: A review of assessing the accuracy of classifications of remotely sensed data, Remote sensing of environment, 37, 35-46, https://doi.org/10.1016/0034-4257(91)90048-B, 1991.

Crisóstomo de Castro Filho, H., Abílio de Carvalho Júnior, O., Ferreira de Carvalho, O. L., Pozzobon de Bem, P., dos Santos de Moura, R., Olino de Albuquerque, A., Rosa Silva, C., Guimarães Ferreira, P. H., Fontes Guimarães, R., and Trancoso Gomes, R. A.: Rice Crop Detection Using LSTM, Bi-LSTM, and Machine Learning Models from Sentinel-1 Time Series, Remote Sensing, 12, 10.3390/rs12162655, 2020.

Cué La Rosa, L. E., Queiroz Feitosa, R., Nigri Happ, P., Del'Arco Sanches, I., and Ostwald Pedro da Costa, G. A.: Combining Deep Learning and Prior Knowledge for Crop Mapping in Tropical Regions from Multitemporal SAR Image Sequences, Remote Sensing, 11, 10.3390/rs11172029, 2019.

Desa, U.: Transforming our world: The 2030 agenda for sustainable development, https://sustainabledevelopment.un.org/post2015/transformingourworld/publication, 2016.

Dong, J., Xiao, X., Menarguez, M. A., Zhang, G., Qin, Y., Thau, D., Biradar, C., and Moore, B., 3rd: Mapping paddy rice planting area in northeastern Asia with Landsat 8 images, phenology-based algorithm and Google Earth Engine, Remote Sens Environ, 185, 142-154, 10.1016/j.rse.2016.02.016, 2016a.

Dong, J., Xiao, X., Zhang, G., Menarguez, M., Choi, C., Qin, Y., Luo, P., Zhang, Y., and Moore, B.: Northward expansion of paddy rice in northeastern Asia during 2000–2014, Geophysical research letters, 43, 3754-3761, 10.1002/2016GL068191, 2016b.

Dong, J., Xiao, X., Kou, W., Qin, Y., Zhang, G., Li, L., Jin, C., Zhou, Y., Wang, J., Biradar, C., Liu, J., and Moore, B.: Tracking the dynamics of paddy rice planting area in 1986–2010 through time series Landsat images and phenology-based algorithms, Remote Sensing of Environment, 160, 99-113, 10.1016/j.rse.2015.01.004, 2015.

Draper, N. R. and Smith, H.: Applied regression analysis, John Wiley & Sons, https://doi.org/10.1002/bimj.19690110613, 1998.

FAO:World rice production (Crops > Items > Rice, paddy): https://www.fao.org/faostat/en/#data/QCL, last access: 7/11/2022.

FAOSTAT: Statistical Database of the Food and Agricultural Organization of the United Nations., https://www.fao.org/statistics/en/, 2010.

Filipponi, F.: Sentinel-1 GRD Preprocessing Workflow, 3rd International Electronic Conference on Remote Sensing, 10.3390/ecrs-3-06201, 2019.

Godfray, H. C., Beddington, J. R., Crute, I. R., Haddad, L., Lawrence, D., Muir, J. F., Pretty, J., Robinson, S., Thomas, S. M., and Toulmin, C.: Food security: the challenge of feeding 9 billion people, Science, 327, 812-818, 10.1126/science.1185383, 2010.

Guan, X., Huang, C., Liu, G., Meng, X., and Liu, Q.: Mapping rice cropping systems in Vietnam using an NDVI-based time-series similarity measurement based on DTW distance, Remote Sensing, 8, 19, 10.3390/rs8010019, 2016.

Gumma, M. K., Nelson, A., Thenkabail, P. S., and Singh, A. N.: Mapping rice areas of South Asia using MODIS multitemporal data, Journal of applied remote sensing, 5, 053547, 10.1117/1.3619838, 2011a.

Gumma, M. K., Gauchan, D., Nelson, A., Pandey, S., and Rala, A.: Temporal changes in rice-growing area and their impact on livelihood over a decade: A case study of Nepal, Agriculture, Ecosystems & Environment, 142, 382-392, 10.1016/j.agee.2011.06.010, 2011b.

Gumma, M. K., Thenkabail, P. S., Maunahan, A., Islam, S., and Nelson, A.: Mapping seasonal rice cropland extent and area in the high cropping intensity environment of Bangladesh using MODIS 500 m data for the year 2010, ISPRS Journal of Photogrammetry and Remote Sensing, 91, 98-113, 10.1016/j.isprsjprs.2014.02.007, 2014.

Han, J., Zhang, Z., Luo, Y., Cao, J., Zhang, L., Cheng, F., Zhuang, H., Zhang, J., and Tao, F.: NESEA-Rice10: high-resolution annual paddy rice maps for Northeast and Southeast Asia from 2017 to 2019, Earth System Science Data, 13, 5969-5986, 10.5194/essd-13-5969-2021, 2021.

Han, J., Zhang, Z., Luo, Y., Cao, J., Zhang, L., Zhuang, H., Cheng, F., Zhang, J., and Tao, F.: Annual paddy rice planting area and cropping intensity datasets and their dynamics in the Asian monsoon region from 2000 to 2020, Agricultural Systems, 200, 10.1016/j.agsy.2022.103437, 2022.

Hoang-Phi, P., Nguyen-Kim, T., Nguyen-Van-Anh, V., Lam-Dao, N., Le-Van, T., and Pham-Duy, T.: Rice yield estimation in An Giang province, the Vietnamese Mekong Delta using Sentinel-1 radar remote sensing data, IOP Conference Series: Earth and Environmental Science, 652, 012001, 10.1088/1755-1315/652/1/012001, 2021.

Huang, X., Wang, J., Shang, J., Liao, C., and Liu, J.: Application of polarization signature to land cover scattering mechanism analysis and classification using multi-temporal C-band polarimetric RADARSAT-2 imagery, Remote Sensing of Environment, 193, 11-28, 10.1016/j.rse.2017.02.014, 2017.

Inoue, S., Ito, A., and Yonezawa, C.: Mapping Paddy fields in Japan by using a Sentinel-1 SAR time series supplemented by Sentinel-2 images on Google Earth Engine, Remote Sensing, 12, 1622, doi:10.3390/rs12101622, 2020.

Ioffe, S. and Szegedy, C.: Batch Normalization: Accelerating Deep Network Training by Reducing Internal Covariate Shift, ArXiv, abs/1502.03167, https://doi.org/10.48550/arXiv.1502.03167, 2015.

Jin, X., Kumar, L., Li, Z., Feng, H., Xu, X., Yang, G., and Wang, J.: A review of data assimilation of remote sensing and crop models, European Journal of Agronomy, 92, 141-152, 10.1016/j.eja.2017.11.002, 2018.

Johnson, D. M. and Mueller, R.: The 2009 cropland data layer, Photogramm. Eng. Remote Sens, 76, 1201-1205, 2010.

Kang, J., Yang, X., Wang, Z., Huang, C., and Wang, J.: Collaborative Extraction of Paddy Planting Areas with Multi-Source Information Based on Google Earth Engine: A Case Study of Cambodia, Remote Sensing, 14, 10.3390/rs14081823, 2022.

Kuenzer, C. and Knauer, K.: Remote sensing of rice crop areas, International Journal of Remote Sensing, 34, 2101-2139, 10.1080/01431161.2012.738946, 2012.

Laborte, A. G., Gutierrez, M. A., Balanza, J. G., Saito, K., Zwart, S. J., Boschetti, M., Murty, M. V. R., Villano, L., Aunario, J. K., Reinke, R., Koo, J., Hijmans, R. J., and Nelson, A.: RiceAtlas, a spatial database of global rice calendars and production, Sci Data, 4, 170074, 10.1038/sdata.2017.74, 2017.

Li, H., Fu, D., Huang, C., Su, F., Liu, Q., Liu, G., and Wu, S.: An Approach to High-Resolution Rice Paddy Mapping Using Time-Series Sentinel-1 SAR Data in the Mun River Basin, Thailand, Remote Sensing, 12, 10.3390/rs12233959, 2020.

Lin, C., Zhong, L., Song, X.-P., Dong, J., Lobell, D. B., and Jin, Z.: Early-and in-season crop type mapping without current-year ground truth: Generating labels from historical information via a topology-based approach, Remote Sensing of Environment, 274, 112994, https://doi.org/10.1016/j.rse.2022.112994, 2022.

Liu, C.-a., Chen, Z.-x., Shao, Y., Chen, J.-s., Hasi, T., and Pan, H.-z.: Research advances of SAR remote sensing for agriculture applications: A review, Journal of Integrative Agriculture, 18, 506-525, 10.1016/s2095-3119(18)62016-7, 2019.

Liu, R., Zhang, G., Dong, J., Zhou, Y., You, N., He, Y., and Xiao, X.: Evaluating Effects of Medium-Resolution Optical Data Availability on Phenology-Based Rice Mapping in China, Remote Sensing, 14, 10.3390/rs14133134, 2022.

Liu, Z., Hu, Q., Tan, J., and Zou, J.: Regional scale mapping of fractional rice cropping change using a phenology-based temporal mixture analysis, International Journal of Remote Sensing, 40, 2703-2716, 10.1080/01431161.2018.1530812, 2018.

Luo, Y., Zhang, Z., Li, Z., Chen, Y., Zhang, L., Cao, J., and Tao, F.: Identifying the spatiotemporal changes of annual harvesting areas for three staple crops in China by integrating multi-data sources, Environmental Research Letters, 15, 10.1088/1748-9326/ab80f0, 2020.

Manjunath, K., More, R. S., Jain, N., Panigrahy, S., and Parihar, J.: Mapping of rice-cropping pattern and cultural type using remote-sensing and ancillary data: A case study for South and Southeast Asian countries, International Journal of Remote Sensing, 36, 6008-6030, https://doi.org/10.1080/01431161.2015.1110259, 2015.

Mansaray, L. R., Kabba, V. T. S., Zhang, L., and Bebeley, H. A.: Optimal multi-temporal Sentinel-1A SAR imagery for paddy rice field discrimination; a recommendation for operational mapping initiatives, Remote Sensing Applications: Society and Environment, 22, 10.1016/j.rsase.2021.100533, 2021.

McHugh, M. L.: Interrater reliability: the kappa statistic, Biochemia medica, 22, 276-282, https://doi.org/10.11613/BM.2012.031, 2012.

Mosleh, M. K., Hassan, Q. K., and Chowdhury, E. H.: Application of remote sensors in mapping rice area and forecasting its production: a review, Sensors (Basel), 15, 769-791, 10.3390/s150100769, 2015.

Ndikumana, E., Ho Tong Minh, D., Baghdadi, N., Courault, D., and Hossard, L.: Deep Recurrent Neural Network for Agricultural Classification using multitemporal SAR Sentinel-1 for Camargue, France, Remote Sensing, 10, 10.3390/rs10081217, 2018.

Nelson, A. and Gumma, M. K.: A map of lowland rice extent in the major rice growing countries of Asia, IRRI [dataset], http://irri.org/our-work/research/policy-and-markets/mapping.37, 2015.

Nelson, A., Setiyono, T., Rala, A., Quicho, E., Raviz, J., Abonete, P., Maunahan, A., Garcia, C., Bhatti, H., Villano, L., Thongbai, P., Holecz, F., Barbieri, M., Collivignarelli, F., Gatti, L., Quilang, E., Mabalay, M., Mabalot, P., Barroga, M., Bacong, A., Detoito, N., Berja, G., Varquez, F., Wahyunto, Kuntjoro, D., Murdiyati, S., Pazhanivelan, S., Kannan, P., Mary, P., Subramanian, E., Rakwatin, P., Intrman, A., Setapayak, T., Lertna, S., Minh, V., Tuan, V., Duong, T., Quyen, N., Van Kham, D., Hin, S., Veasna, T., Yadav, M., Chin, C., and Ninh, N.: Towards an Operational SAR-Based Rice Monitoring System in Asia: Examples from 13 Demonstration Sites across Asia in the RIICE Project, Remote Sensing, 6, 10773-10812, 10.3390/rs61110773, 2014.

Nguyen, D. B. and Wagner, W.: European Rice Cropland Mapping with Sentinel-1 Data: The Mediterranean Region Case Study, Water, 9, 10.3390/w9060392, 2017.

Ni, R., Tian, J., Li, X., Yin, D., Li, J., Gong, H., Zhang, J., Zhu, L., and Wu, D.: An enhanced pixel-based phenological feature for accurate paddy rice mapping with Sentinel-2 imagery in Google Earth Engine, ISPRS Journal of Photogrammetry and Remote Sensing, 178, 282-296, 10.1016/j.isprsjprs.2021.06.018, 2021.
Orynbaikyzy, A., Gessner, U., and Conrad, C.: Crop type classification using a combination of optical and radar remote sensing data: a review, International Journal of Remote Sensing, 40, 6553-6595, 10.1080/01431161.2019.1569791, 2019.
Pan, B., Zheng, Y., Shen, R., Ye, T., Zhao, W., Dong, J., Ma, H., and Yuan, W.: High Resolution Distribution Dataset of Double-Season Paddy Rice in China, Remote Sensing, 13, 10.3390/rs13224609, 2021.
Phan, D. C., Trung, T. H., Truong, V. T., Sasagawa, T., Vu, T. P. T., Bui, D. T., Hayashi, M., Tadono, T., and Nasahara, K. N.: First comprehensive quantification of annual land use/cover from 1990 to 2020 across mainland Vietnam, Sci Rep, 11, 9979, 10.1038/s41598-021-89034-5, 2021.
Qiu, B., Hu, X., Chen, C., Tang, Z., Yang, P., Zhu, X., Yan, C., and Jian, Z.: Maps of cropping patterns in China during 2015-2021, Sci Data, 9, 479, 10.1038/s41597-022-01589-8, 2022.
Ronneberger, O., Fischer, P., and Brox, T.: U-Net: Convolutional Networks for Biomedical Image Segmentation, ArXiv, abs/1505.04597, https://doi.org/10.48550/arXiv.1505.04597, 2015.
Shew, A. M. and Ghosh, A.: Identifying Dry-Season Rice-Planting Patterns in Bangladesh Using the Landsat Archive, Remote Sensing, 11, 10.3390/rs11101235, 2019.
Singha, M., Dong, J., Zhang, G., and Xiao, X.: High resolution paddy rice maps in cloud-prone Bangladesh and Northeast India using Sentinel-1 data, Sci Data, 6, 26, 10.1038/s41597-019-0036-3, 2019.
Soh, N. C., Shah, R. M., Giap, S. G. E., Setiawan, B. I., and Minasny, B.: High-Resolution Mapping of Paddy Rice Extent and Growth Stages across Peninsular Malaysia Using a Fusion of Sentinel-1 and 2 Time Series Data in Google Earth Engine, Remote Sensing, 14, 1875, 10.3390/rs14081875, 2022.
Sun, C., Zhang, H., Xu, L., Wang, C., and Li, L.: Rice Mapping Using a BiLSTM-Attention Model from Multitemporal Sentinel-1 Data, Agriculture, 11, 977, 10.3390/agriculture11100977, 2021.
Sun, C., Zhang, H., Ge, J., Wang, C., Li, L., and Xu, L.: Rice Mapping in a Subtropical Hilly Region Based on Sentinel-1 Time Series Feature Analysis and the Dual Branch BiLSTM Model, Remote Sensing, 14, 10.3390/rs14133213, 2022a.
Sun, C., Zhang, H., Xu, L., Ge, J., Jiang, J., Zuo, L., and Wang, C.: 20 m Annual Paddy Rice Map for Mainland Southeast Asia Using Sentinel-1 SAR Data (1) [dataset], https://doi.org/10.5281/zenodo.7315076, 2022b.
Sun, H.-s., Huang, J.-f., Huete, A. R., Peng, D.-l., and Zhang, F.: Mapping paddy rice with multi-date moderate-resolution imaging spectroradiometer (MODIS) data in China, Journal of Zhejiang University-Science A, 10, 1509-1522, 10.1631/jzus.A0820536, 2009.
Thenkabail, P. S., Biradar, C. M., Noojipady, P., Dheeravath, V., Li, Y., Velpuri, M., Gumma, M., Gangalakunta, O. R. P., Turral, H., and Cai, X.: Global irrigated area map (GIAM), derived from remote sensing, for the end of the last millennium, International Journal of Remote Sensing, 30, 3679-3733, 10.1080/01431160802698919, 2009.
Torbick, N., Chowdhury, D., Salas, W., and Qi, J.: Monitoring Rice Agriculture across Myanmar Using Time Series Sentinel-1 Assisted by Landsat-8 and PALSAR-2, Remote Sensing, 9, 10.3390/rs9020119, 2017.
Torres, R., Snoeij, P., Geudtner, D., Bibby, D., Davidson, M., Attema, E., Potin, P., Rommen, B., Floury, N., and Brown, M.: GMES Sentinel-1 mission, Remote sensing of environment, 120, 9-24, 10.1016/j.rse.2011.05.028, 2012.
Tsokas, A., Rysz, M., Pardalos, P. M., and Dipple, K.: SAR data applications in earth observation: An overview, Expert Systems with Applications, 205, 10.1016/j.eswa.2022.117342, 2022.
Vapnik, V. N.: An overview of statistical learning theory, IEEE transactions on neural networks, 10, 988-999, 10.1109/72.788640, 1999.
Wei, J., Cui, Y., Luo, W., and Luo, Y.: Mapping Paddy Rice Distribution and Cropping Intensity in China from 2014 to 2019 with Landsat Images, Effective Flood Signals, and Google Earth Engine, Remote Sensing, 14, 759, 10.3390/rs14030759, 2022.
Wei, P., Chai, D., Lin, T., Tang, C., Du, M., and Huang, J.: Large-scale rice mapping under different years based on time-series Sentinel-1 images using deep semantic segmentation model, ISPRS Journal of Photogrammetry and Remote Sensing, 174, 198-214, 10.1016/j.isprsjprs.2021.02.011, 2021.
Wei, S., Zhang, H., Wang, C., Wang, Y., and Xu, L.: Multi-Temporal SAR Data Large-Scale Crop Mapping Based on U-Net Model, Remote Sensing, 11, 10.3390/rs11010068, 2019.
Weiss, M., Jacob, F., and Duveiller, G.: Remote sensing for agricultural applications: A meta-review, Remote Sensing of Environment, 236, 10.1016/j.rse.2019.111402, 2020.
Xiao, X., Boles, S., Frolking, S., Li, C., Babu, J. Y., Salas, W., and Moore III, B.: Mapping paddy rice agriculture in South and Southeast Asia using multi-temporal MODIS images, Remote sensing of Environment, 100, 95-113, 10.1016/j.rse.2005.10.004, 2006.
Xiao, X., Boles, S., Liu, J., Zhuang, D., Frolking, S., Li, C., Salas, W., and Moore III, B.: Mapping paddy rice agriculture in southern China using multi-temporal MODIS images, Remote sensing of environment, 95, 480-492, https://doi.org/10.1016/j.rse.2004.12.009, 2005.
Xin, F., Xiao, X., Dong, J., Zhang, G., Zhang, Y., Wu, X., Li, X., Zou, Z., Ma, J., Du, G., Doughty, R. B., Zhao, B., and Li, B.: Large increases of paddy rice area, gross primary production, and grain production in Northeast China during 2000-2017, Sci Total Environ, 711, 135183, 10.1016/j.scitotenv.2019.135183, 2020.

Xu, L., Zhang, H., Wang, C., Wei, S., Zhang, B., Wu, F., and Tang, Y.: Paddy Rice Mapping in Thailand Using Time-Series Sentinel-1 Data and Deep Learning Model, Remote Sensing, 13, 3994, 10.3390/rs13193994, 2021.

Yang, L., Wang, L., Huang, J., Mansaray, L. R., and Mijiti, R.: Monitoring policy-driven crop area adjustments in northeast China using Landsat-8 imagery, International Journal of Applied Earth Observation and Geoinformation, 82, 10.1016/j.jag.2019.06.002, 2019.

Yang, L., Huang, R., Huang, J., Lin, T., Wang, L., Mijiti, R., Wei, P., Tang, C., Shao, J., Li, Q., and Du, X.: Semantic Segmentation Based on Temporal Features: Learning of Temporal-Spatial Information From Time-Series SAR Images for Paddy Rice Mapping, IEEE Transactions on Geoscience and Remote Sensing, 1-16, 10.1109/tgrs.2021.3099522, 2021.

You, N. and Dong, J.: Examining earliest identifiable timing of crops using all available Sentinel 1/2 imagery and Google Earth Engine, ISPRS Journal of Photogrammetry and Remote Sensing, 161, 109-123, 10.1016/j.isprsjprs.2020.01.001, 2020.

You, N., Dong, J., Huang, J., Du, G., Zhang, G., He, Y., Yang, T., Di, Y., and Xiao, X.: The 10-m crop type maps in Northeast China during 2017-2019, Sci Data, 8, 41, 10.1038/s41597-021-00827-9, 2021.

Yu, Q., You, L., Wood-Sichra, U., Ru, Y., Joglekar, A. K. B., Fritz, S., Xiong, W., Lu, M., Wu, W., and Yang, P.: A cultivated planet in 2010 – Part 2: The global gridded agricultural-production maps, Earth System Science Data, 12, 3545-3572, 10.5194/essd-12-3545-2020, 2020.

Yuan, S., Stuart, A. M., Laborte, A. G., Rattalino Edreira, J. I., Dobermann, A., Kien, L. V. N., Thúy, L. T., Paothong, K., Traesang, P., Tint, K. M., San, S. S., Villafuerte, M. Q., Quicho, E. D., Pame, A. R. P., Then, R., Flor, R. J., Thon, N., Agus, F., Agustiani, N., Deng, N., Li, T., and Grassini, P.: Southeast Asia must narrow down the yield gap to continue to be a major rice bowl, Nature Food, 3, 217-226, 10.1038/s43016-022-00477-z, 2022.

Zanaga, D., Van De Kerchove, R., De Keersmaecker, W., Souverijns, N., Brockmann, C., Quast, R., Wevers, J., Grosu, A., Paccini, A., and Vergnaud, S.: ESA WorldCover 10 m 2020 v100, https://doi.org/10.5281/zenodo.5571936, 2021.

Zhang, G., Xiao, X., Biradar, C. M., Dong, J., Qin, Y., Menarguez, M. A., Zhou, Y., Zhang, Y., Jin, C., Wang, J., Doughty, R. B., Ding, M., and Moore, B., 3rd: Spatiotemporal patterns of paddy rice croplands in China and India from 2000 to 2015, Sci Total Environ, 579, 82-92, 10.1016/j.scitotenv.2016.10.223, 2017.

Zhang, X., Wu, B., Ponce-Campos, G., Zhang, M., Chang, S., and Tian, F.: Mapping up-to-Date Paddy Rice Extent at 10 M Resolution in China through the Integration of Optical and Synthetic Aperture Radar Images, Remote Sensing, 10, 10.3390/rs10081200, 2018.

Zhao, R., Li, Y., and Ma, M.: Mapping Paddy Rice with Satellite Remote Sensing: A Review, Sustainability, 13, 10.3390/su13020503, 2021.